

CRAFT: Aligning Diffusion Models with Fine-Tuning Is Easier Than You Think

Zening Sun^{1*} Zhengpeng Xie^{1*} Lichen Bai¹ Shitong Shao¹ Shuo Yang² Zeke Xie^{1†}
¹ HKUST (GZ) ² HIT (SZ)

Abstract

Aligning Diffusion models has achieved remarkable breakthroughs in generating high-quality, human preference-aligned images. Existing techniques, such as supervised fine-tuning (SFT) and DPO-style preference optimization, have become principled tools for fine-tuning diffusion models. However, SFT relies on high-quality images that are costly to obtain, while DPO-style methods depend on large-scale preference datasets, which are often inconsistent in quality. Beyond data dependency, these methods are further constrained by computational inefficiency. To address these two challenges, we propose Composite Reward Assisted Fine-Tuning (CRAFT), a lightweight yet powerful fine-tuning paradigm that requires significantly reduced training data while maintaining computational efficiency. It first leverages a Composite Reward Filtering (CRF) technique to construct a high-quality and consistent training dataset and then perform an enhanced variant of SFT. We also theoretically prove that CRAFT actually optimizes the lower bound of group-based reinforcement learning, establishing a principled connection between SFT with selected data and reinforcement learning. Our extensive empirical results demonstrate that CRAFT with only 100 samples can easily outperform recent SOTA preference optimization methods with thousands of preference-paired samples. Moreover, CRAFT can even achieve 11-220× faster convergences than the baseline preference optimization methods, highlighting its extremely high efficiency.

1. Introduction

Recent advances in diffusion models (DMs) [6, 36] have significantly propelled text-to-image (T2I) generation, achieving substantial improvements in visual fidelity and text-image alignment [11, 21, 27]. Despite these breakthroughs, diffusion models are typically pretrained on noisy large-scale, web-sourced datasets [25, 28, 29]. Therefore, their outputs often fail to align with human preferences for aesthetics and instruction-following, highlighting a need for

*Equal contribution.

†Corresponding author.

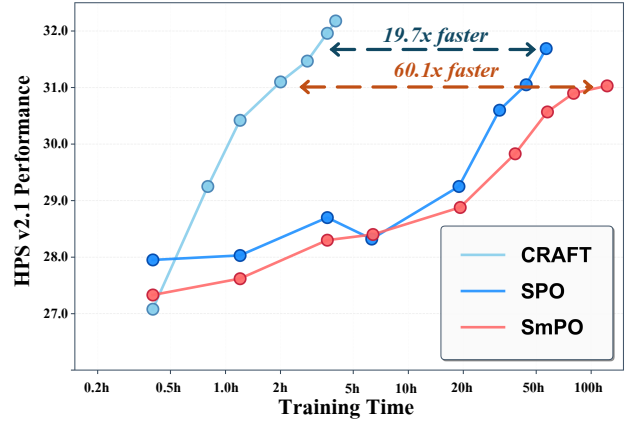


Figure 1. **Training Efficiency Comparison.** Compared to SPO and SmPO, CRAFT reaches the same HPSv2.1 performance with 19.7× and 60.1× faster training time respectively, and further achieves superior final performance, demonstrating a dual advantage in both training speed and final generation quality.

effective alignment. Inspired by the success of post-training techniques in large language models (LLMs) [20, 24, 38], numerous recent studies have adapted these methods to fine-tune diffusion models for human preference alignment.

Existing post-training approaches present a trade-off between data requirements and computational cost. Supervised Fine-Tuning (SFT), while computationally lean, hinges on access to exceptionally high-quality datasets that are scarce and expensive to curate. Inspired by the success of Direct Preference Optimization (DPO) in LLMs [24], Diffusion-DPO [37] adapted this paradigm to fine-tune diffusion models. This offline approach achieves strong alignment and inspired many DPO-style methods. A prominent example is SmPO [19], which builds upon the DPO framework by incorporating smoothed reward signal processing. While effective, the fundamental limitation of these offline DPO-style approaches is their reliance on large-scale data. Alternatively, many online methods, exemplified by SPO [15], generate preference pairs dynamically at each denoising step. Although this avoids reliance on large-scale datasets, it incurs immense computational overhead from

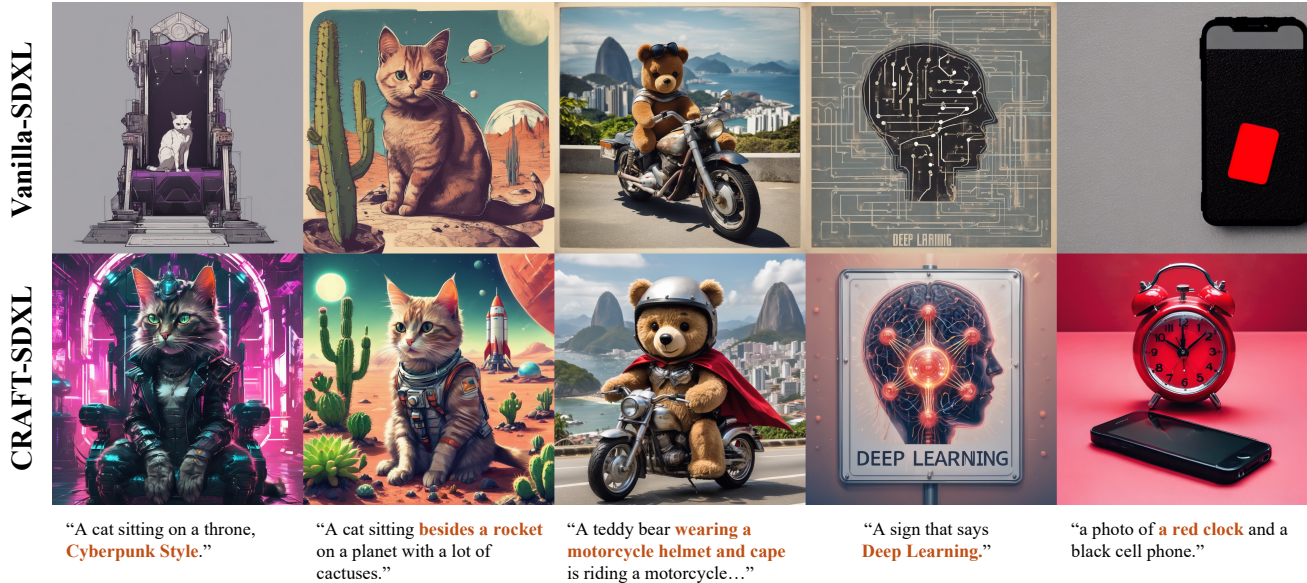


Figure 2. **Qualitative Improvements over Vanilla SDXL.** We present CRAFT, an efficient and effective fine-tuning method designed to enhance diffusion models’ alignment with human preference. The top row displays images generated by the base Vanilla-SDXL model, while the bottom row shows results generated by our CRAFT-finetuned model (CRAFT-SDXL). The comparison clearly shows that CRAFT-SDXL excels at complex instruction following and compositional reasoning, demonstrating significant superiority in adhering to diverse stylistic concepts (e.g., “Cyberpunk Style”), accurately generating specified objects and their attributes (e.g., the position of the cat “beside a rocket” and the teddy bear “wearing a helmet and cape”), and precisely rendering on-image text (e.g., “Deep Learning”).

repeated online sampling and evaluation. Consequently, aligning diffusion models remains challenging due to the scarcity of high-quality data and the high computational cost of existing methods. Therefore, a fine-tuning approach that is both data-efficient and computationally lightweight is important for the future of diffusion model alignment.

To address these two challenges, we propose **Composite Reward Assisted Fine-Tuning (CRAFT)**, a simple yet effective framework for aligning diffusion models efficiently with as few as 100 samples. CRAFT introduces a self-curated and computationally efficient training paradigm that fine-tunes models through an enhanced SFT guided by a composite reward function. Specifically, we leverage our Composite Reward Filtering strategy, which enables the automatic selection of representative, distribution-consistent training samples without reliance on external high-quality datasets or data distilled from stronger models. Moreover, we theoretically prove that CRAFT can be interpreted as a lower bound of group-based reinforcement learning, providing a principled bridge between supervised fine-tuning and reinforcement learning from human feedback.

We use CRAFT to fine-tune Stable Diffusion v1.5 and Stable Diffusion XL using only **100** samples. As illustrated in Fig. 1, CRAFT reaches the same HPSv2.1 performance 19.7× faster than SPO and 60.1× faster than SmPO and achieves the best HPSv2.1 performance. Moreover, as

shown in Fig. 2 and Fig. 4, CRAFT substantially enhances the generative quality and aesthetic fidelity. Notably, our composite reward function does not include ImageReward and MPS, yet CRAFT attains the highest scores on SDXL and SD1.5 across all tests (see Table 2 and Table 3). Our main contributions are summarized as follows:

- (i) We propose CRAFT, a simple yet effective alignment framework that eliminates the dependence on large-scale preference datasets while reducing computational cost, achieving strong preference alignment with 100 samples.
- (ii) We theoretically prove that our CRAFT can be interpreted as a lower-bound optimization of group-based reinforcement learning, establishing a principled connection between supervised fine-tuning and reinforcement learning.
- (iii) Extensive experiments on SD1.5 and SDXL demonstrate that our CRAFT achieves up to 11–220× faster training while maintaining superior preference alignment, confirming the efficiency and effectiveness of our approach.

2. Related Work

Text-to-Image Diffusion Models. Diffusion models (DMs) [6, 16, 35, 36, 43] have emerged as the dominant paradigm for text-to-image (T2I) generation, surpassing earlier models such as GANs [9, 26] in visual fidelity. Building upon the foundational advances in denoising diffusion probabilistic models, DALL-E [25], Imagen [28],

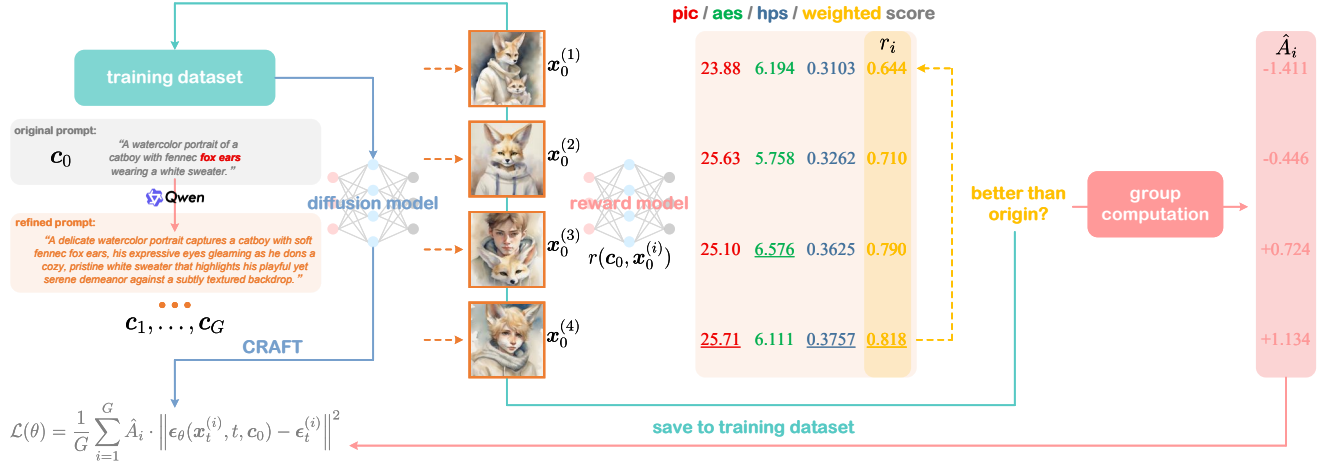


Figure 3. **The overall pipeline of our method** mainly consists of three stages: (i) data construction, (ii) composite reward filtering, and (iii) weighted SFT fine-tuning.

and Stable Diffusion [21, 27] introduced powerful text-conditioning mechanisms and latent-space diffusion, enabling high-resolution and prompt-controllable image synthesis. However, although producing visually compelling results, current T2I diffusion models often fail to align closely with human preferences [14, 37, 43]. This misalignment primarily arises from their training stage, which rely on large-scale but noisy datasets (e.g., LAION-5B [29]) and simple reconstruction losses [6, 27]. In this work, we introduce a simple yet effective method CRAFT to make fine-tuning diffusion models easier.

Aligning Diffusion Models. Inspired by post-training techniques in large language models (LLMs) such as SFT and RLHF, diffusion model alignment has recently gained increasing attention. Supervised Fine-Tuning (SFT) directly fine-tunes diffusion models on curated text-image pairs to improve prompt adherence and visual fidelity, yet its reliance on high-quality data limits practicality. RL-based alignment adapts RLHF methods by framing denoising as a policy optimization process. Approaches such as DDPO [3], DPOK [4], and GRPO-style extensions [17, 34, 42] introduce log-probability based supervision for stability, but remain computationally expensive and often unstable under sparse or noisy rewards. Recently, preference optimization has emerged as a more practical alternative for aligning diffusion models with human judgments. Direct Preference Optimization (DPO) [24] replaces explicit reward modeling with pairwise preference supervision, achieving alignment comparable to RLHF in LLMs. This concept was later extended to diffusion models via Diffusion-DPO [37], which directly optimizes generation quality using preference pairs. Building on this paradigm, subsequent variants, such as DSPO [48], SPO [15], and

SmPO [19] explore score coupling, step-aware rewards, and reward smoothing for improved stability and fidelity.

3. Methodology

In this section, we first build some theoretical insights in Section 3.1, introduce *Composite Reward Filtering* (CRF) technique in Section 3.2, and in Section 3.3 we propose our practical fine-tuning algorithm called *Composite Reward Assisted Fine-Tuning* (CRAFT).

3.1. Formulation and Theoretical Insights

We begin by introducing some basic formulation under reinforcement learning settings. Suppose we have a diffusion model $p_{\theta}(x_0|c)$, where $c \in \mathcal{D}_c$ is the prompt, and x_0 is the clean image. Given a reward model $r(c, x_0)$, our goal is to optimize the following objective:

$$\begin{aligned} J(\theta) &= \mathbb{E}_{c \sim \mathcal{D}_c, x_0 \sim p_{\theta}(\cdot|c)} [r(c, x_0)] \\ &= \mathbb{E}_{c \sim \mathcal{D}_c, x_0 \sim p_{\theta_{\text{old}}}(\cdot|c)} \left[\frac{p_{\theta}(x_0|c)}{p_{\theta_{\text{old}}}(x_0|c)} \cdot r(c, x_0) \right], \end{aligned} \quad (1)$$

where we use *importance sampling* to decouple the behavior policy $p_{\theta_{\text{old}}}$ and the target policy p_{θ} . While traditional RLHF formulations employ KL regularization to prevent reward over-optimization, we omit this component since prior works indicate only minimal performance differences [42]. Then, motivated by the core idea of group-based fine-tuning technique [34], we can further approximate this objective using the *Monte Carlo* method as follows:

$$\hat{J}(\theta) = \mathbb{E}_{c \sim \mathcal{D}_c, \{x_0^{(i)}\}_{i=1}^G \sim p_{\theta_{\text{old}}}(\cdot|c)} \left[\frac{1}{G} \sum_{i=1}^G \frac{p_{\theta}(x_0^{(i)}|c)}{p_{\theta_{\text{old}}}(x_0^{(i)}|c)} \cdot \hat{A}_i \right], \quad (2)$$

where $\hat{A}_i = (r(\mathbf{c}, \mathbf{x}_0^{(i)}) - \text{mean}) / (\text{std} + \epsilon)$, mean and std represent the mean and standard deviation of the group rewards $\{r(\mathbf{c}, \mathbf{x}_0^{(i)})\}_{i=1}^G$, and $\epsilon > 0$ is a small constant for numerical stability.

We are now ready to present the main theoretical result of this paper:

Theorem 3.1 *Given a Text-to-Image (T2I) diffusion model $p_\theta(\mathbf{x}_0|\mathbf{c})$, for any gradient direction g with a small learning rate¹ $\eta \rightarrow 0$ ($\theta = \theta_{\text{old}} + \eta g$), the following bound holds:*

$$\hat{J}(\theta) \geq C - \mathbb{E}_{\substack{\mathbf{c} \sim \mathcal{D}_{\mathbf{c}}, \\ \{\mathbf{x}_0^{(i)}\}_{i=1}^G \sim p_{\theta_{\text{old}}}(\cdot|\mathbf{c}), \\ t \sim \text{Uniform}\{1, \dots, T\}, \\ \epsilon_t^{(i)} \sim \mathcal{N}(0, I)}} \left[\frac{1}{G} \sum_{i=1}^G \hat{A}_i w(t) \cdot \left\| \epsilon_\theta(\mathbf{x}_t^{(i)}, t, \mathbf{c}) - \epsilon_t^{(i)} \right\|^2 \right],$$

where ϵ_θ is the noise predictive model of p_θ , and C is a constant that do not depends on θ .

The detailed proof of Theorem 3.1 is shown in Appendix. Theorem 3.1 establishes a principled connection between *group-based RL* and *SFT*. Intuitively, given a batch of data for fine-tuning diffusion models (which can be either model-generated or existing data, corresponding to the *online* and *offline* settings, respectively), the data quality (i.e., the normalized advantage \hat{A}_i) determines the magnitude of the gradient, encouraging the model to generate high-quality images while avoiding low-quality ones.

3.2. Composite Reward Filtering

Data construction. We now provide our data filtering strategy in detail. We randomly sample $n = 10000$ original prompts from the HPD dataset, denoted as $\mathcal{P} = \{\mathbf{c}_1^{(0)}, \mathbf{c}_2^{(0)}, \dots, \mathbf{c}_n^{(0)}\}$, and then we use Qwen-Plus to refine each prompt N times, resulting in a set of refined prompts $\mathcal{P}_{\text{refined}} = \{\mathbf{c}_1^{(1)}, \dots, \mathbf{c}_1^{(N)}, \dots, \mathbf{c}_n^{(1)}, \dots, \mathbf{c}_n^{(N)}\}$. Next, we are ready to build our image dataset. We use the base model $p_\theta(\mathbf{x}_0|\mathbf{c})$ to generate images corresponding to all $n(N+1)$ prompts in set $\mathcal{P} \cup \mathcal{P}_{\text{refined}}$, obtaining the original image dataset $\mathcal{I} = \cup_{\mathbf{c} \in \mathcal{P} \cup \mathcal{P}_{\text{refined}}} \{\mathbf{x}_0 \sim p_\theta(\cdot|\mathbf{c})\}$. We further use the notation $\mathbf{x}_0^{(i,j)} \sim p_\theta(\cdot|\mathbf{c}_i^{(j)})$ to distinguish different images, so $\mathcal{I} = \cup_{i,j} \{\mathbf{x}_0^{(i,j)}\}$, where $i = 1, \dots, n; j = 0, \dots, N$.

Data filtering. To introduce our composite-reward filtering (CRF) strategy, we employ three reward models, they are HPS v2.1 [39], PickScore [10] and AES metric [29]. We denote these models as $r_h(\mathbf{c}, \mathbf{x}_0)$, $r_p(\mathbf{c}, \mathbf{x}_0)$, and $r_a(\mathbf{c}, \mathbf{x}_0)$, respectively. Note that for all images $\mathbf{x}_0 \in \mathcal{I}$, we compute

¹Such assumption is reasonable, since most fine-tuning algorithms set the learning rate between 1e-5 and 1e-6.

Algorithm 1 Composite Reward Assisted Fine-Tuning

Require: Pre-trained Text-to-Image (T2I) diffusion model $p_\theta(\mathbf{x}_0|\mathbf{c})$, original prompt set \mathcal{P} and refined prompt set $\mathcal{P}_{\text{refined}}$, refined image dataset $\mathcal{I} = \cup_{i,j} \{\mathbf{x}_0^{(i,j)}\}$, reward functions r_h, r_p, r_a , reward filtering rules $\tilde{\mathcal{I}} \in \{\mathcal{I}_h, \mathcal{I}_p, \mathcal{I}_a, \mathcal{I}_{ha}, \mathcal{I}_{pa}, \mathcal{I}_{hpa}\}$, batch $b \geq 1$

- 1: **repeat**
- 2: Randomly sample a small batch index $i = k, k + 1, \dots, k + b - 1$ from \mathcal{I}
- 3: Compute group-based advantage:

$$\hat{A}^{(i,j)} = \frac{r_{\text{total}}^{(i,j)} - \text{mean}\{r_{\text{total}}^{(i,1)}, \dots, r_{\text{total}}^{(i,N)}\}}{\text{std}\{r_{\text{total}}^{(i,1)}, \dots, r_{\text{total}}^{(i,N)}\} + \epsilon}$$

- 4: Compute weighted-SFT loss:

$$\mathcal{L}(\theta) := \frac{1}{bN} \sum_{i=k}^{k+b-1} \sum_{j=1}^N$$

$$\hat{A}^{(i,j)} \cdot \left\| \epsilon_\theta(\mathbf{x}_t^{(i,j)}, t, \mathbf{c}_i^{(0)}) - \epsilon_t^{(i,j)} \right\|^2 \cdot \mathbb{I}(\mathbf{x}_0^{(i,j)} \in \tilde{\mathcal{I}})$$

- 5: Optimize \mathcal{L} using gradient decent algorithm
 - 6: **until** converged
-

rewards using their *original* prompts, and refined prompts $\mathcal{P}_{\text{refined}}$ is solely to enhance the diversity of generated images. Formally,

$$r_\xi^{(i,j)} = r_\xi(\mathbf{c}_i^{(0)}, \mathbf{x}_0^{(i,j)}), \quad (3)$$

where $r_\xi^{(i,j)}$ simply denotes the reward for each image $\mathbf{x}_0^{(i,j)}$ given the reward model r_ξ , ξ can be chosen as h, p , or a . With these preparations, we introduce the following three different levels of filtering strategies:

$$\begin{aligned} \mathcal{I}_\xi &= \left\{ \mathbf{x}_0^{(i,j)} \in \mathcal{I} \left| \sum_{j=1}^N \mathbb{I}(r_\xi^{(i,j)} > r_\xi^{(i,0)}) \neq 0 \right. \right\}; \\ \mathcal{I}_{ha} &= \left\{ \mathbf{x}_0^{(i,j)} \in \mathcal{I} \left| \sum_{j=1}^N \prod_{\xi \in \{h,a\}} \mathbb{I}(r_\xi^{(i,j)} > r_\xi^{(i,0)}) \neq 0 \right. \right\}; \\ \mathcal{I}_{pa} &= \left\{ \mathbf{x}_0^{(i,j)} \in \mathcal{I} \left| \sum_{j=1}^N \prod_{\xi \in \{p,a\}} \mathbb{I}(r_\xi^{(i,j)} > r_\xi^{(i,0)}) \neq 0 \right. \right\}; \\ \mathcal{I}_{hpa} &= \left\{ \mathbf{x}_0^{(i,j)} \in \mathcal{I} \left| \sum_{j=1}^N \prod_{\xi \in \{h,p,a\}} \mathbb{I}(r_\xi^{(i,j)} > r_\xi^{(i,0)}) \neq 0 \right. \right\}, \end{aligned} \quad (4)$$

where \mathbb{I} represents the indicator function. In other words, \mathcal{I}_ξ represents the filtering rule for individual rewards: as

long as the refined prompt produces an image with a higher reward than the original one, this batch of generated samples is retained. In contrast, \mathcal{I}_{ha} and \mathcal{I}_{pa} suppose that two types of rewards are simultaneously higher than the originals, while \mathcal{I}_{hpa} requires all three rewards to be higher, making it the strictest rule.

3.3. Composite Reward Assisted Fine-Tuning

Given the theoretical insights from Section 3.1 and the reward filtering techniques described in Section 3.2, we now introduce our fine-tuning algorithm CRAFT, as shown in Algorithm 1.

We use $r_{\text{total}}^{(i,j)}$ to represent the weighted reward when more than one reward model is used for data filtering, i.e., the filtered datasets \mathcal{I}_h , \mathcal{I}_p , \mathcal{I}_{ha} , and \mathcal{I}_{hpa} . We use all the original data and compute the group-based advantage $\hat{A}^{(i,j)}$ for each image $x_0^{(i,j)}$. Then, we calculate the weighted-SFT loss in a small batch. We employ the indicator function $\mathbb{I}(x_0^{(i,j)} \in \tilde{\mathcal{I}})$ to represent that only the filtered data are used for gradient computation. While in Theorem 3.1 the loss coefficient includes the term $w(t)$, in practice previous studies found that removing this term makes the implementation simpler and yields better results [6]. Therefore, we also omit $w(t)$ and use the pure advantage value to represent the gradient magnitude.

4. Experiment

4.1. Experiment Setting

Evaluation. We compare CRAFT with several great fine-tuning approaches, including Diffusion-DPO [24], Diffusion-KTO (for SD1.5) [14], MaPO (for SDXL) [7], SmPO [19], and SPO [15]. For a comprehensive evaluation, we adopt three widely used human preference benchmarks: HPDv2 (3,200 prompts) [39], Parti-Prompts (1,632 prompts) [45], and the Pick-a-Pic validation set (500 prompts) [10]. To further evaluate the general generative capability beyond preference alignment, we test on the Geneval dataset [5], which covers diverse, open-domain prompts to measure image quality, semantic consistency, and visual diversity. We evaluate generated images along three complementary dimensions: (1) human preference alignment, (2) generation quality and (3) aesthetic appeal. For human preference alignment, we adopt HPS v2.1 [39] and employ ImageReward [41] to evaluate generation quality. Finally, we evaluate aesthetic appeal using the AES score [29], which captures visual attractiveness and composition independent of semantic accuracy. As PickScore [10] is trained on the Pick-a-Pic dataset, and most existing alignment methods are optimized on the Pick-a-Pic. To avoid evaluation bias and ensure fair comparison, we exclude PickScore from our evaluation metrics. Furthermore, to demonstrate the generalization of our proposed

composite reward beyond the training distribution, we introduce a newly developed metric: MPS [46]. MPS is a multi-dimensional human preference model that jointly assesses aesthetics, detail quality, semantic alignment, and overall preference, providing a more comprehensive and human-aligned evaluation of text-to-image generation performance. All methods are evaluated under identical generation settings, and we report the average scores across different reward models for each benchmark.

Implementation Details. For data curation, we first refine an initial set of 10,000 prompts from the HPDv2 training set using Qwen-plus [1]. For each refined prompt, we generate a group of $N=4$ images using random seeds. To filter this candidate pool, we apply the \mathcal{I}_{hpa} strategy. The selection and subsequent weighting are guided by a composite reward function r_{total} , which we define as a weighted sum of HPSv2.1, PickScore, and AES with weights of 0.4, 0.4, and 0.2, respectively. The final training dataset is constructed by selecting the highest scoring (text, image) pairs according to this composite reward. We employ AdamW [18] as the optimizer and perform full-parameter fine-tuning on the UNet part of the SD1.5 and SDXL models. We train SD1.5 for 120 steps and SDXL for 200 steps with an effective batch size of 128 and a learning rate of $5e-5$. All experiments are conducted on 8 H100 GPUs.

4.2. Main Results

Qualitative Results. We present a qualitative comparison of CRAFT with baseline methods on SDXL in Figure 4. The results clearly demonstrate CRAFT’s superior ability to follow complex prompts. Our method achieves significant improvements across multiple dimensions including text rendering, stylistic interpretation, compositional reasoning, and object fidelity. For instance, in the first column, CRAFT is the only method that accurately renders the text “CRAFT” with high aesthetic quality, whereas baselines struggle with spelling and coherence. In the second column, when tasked with a stylistic prompt (“Unreal Engine”), CRAFT delivers a more artistically compelling image that captures the requested aesthetic. Furthermore, CRAFT excels at compositional reasoning. It is the only model to correctly interpret the spatial relationship “in front of” in the fourth column, and accurately adheres to both color attributes (“white bottle” and “blue sheep” in column 5) and object counting (“four broccolis” in column 6).

Computational Costs. As illustrated in Table 1 and Figure 1, our CRAFT framework demonstrates a dramatic improvement in computational efficiency. While most baselines rely on vast datasets (up to 928k samples), CRAFT achieves superior alignment using a mere 100 samples. For the fine-tuning stage, CRAFT requires only ~ 4.0 GPU

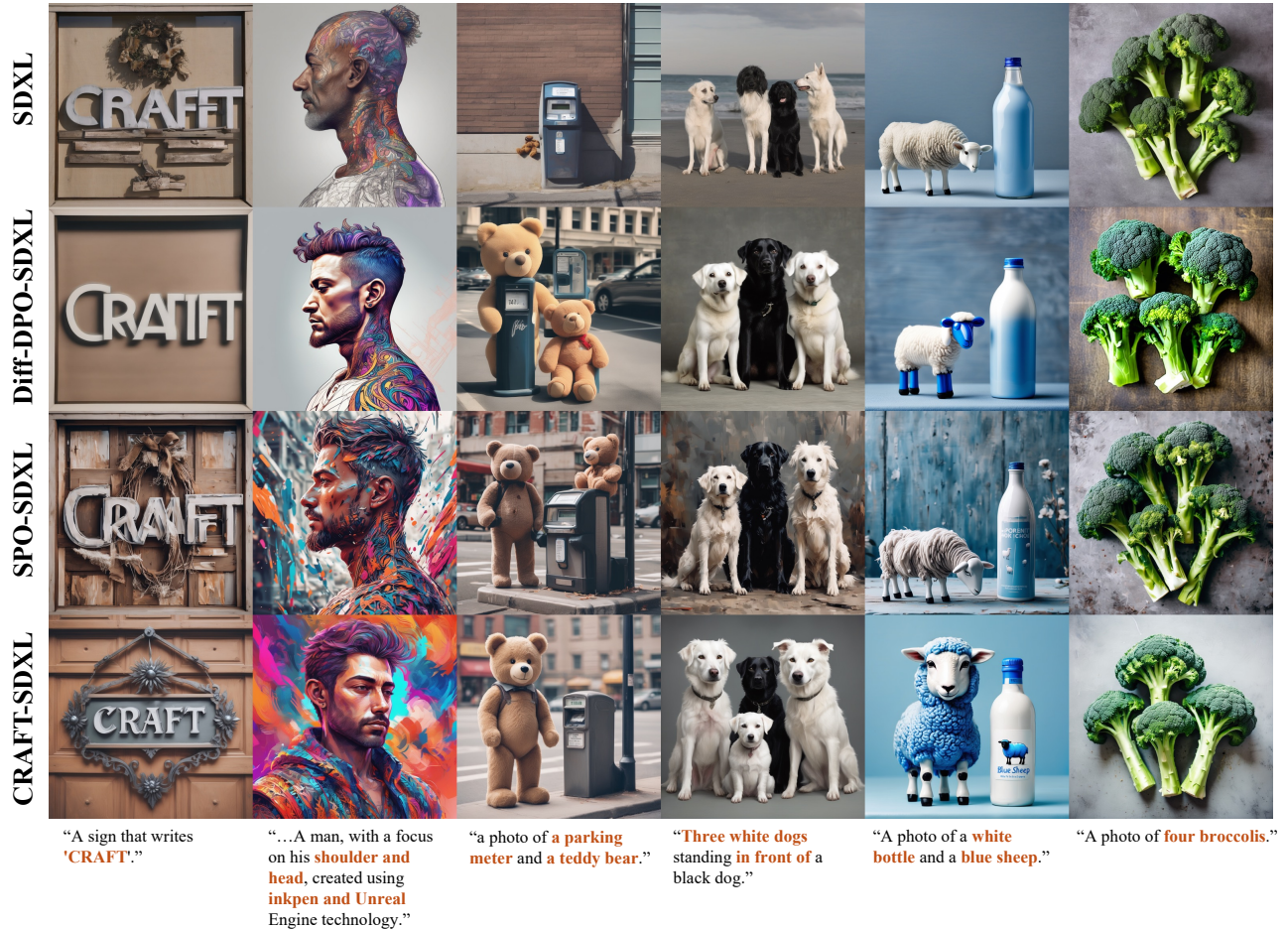


Figure 4. **Qualitative comparison.** We provide a qualitative comparison of CRAFT-Diffusion and other different preference optimization methods (Vanilla, Diff-DPO, SPO) for SDXL. CRAFT-SDXL generates images of superior quality and prompt fidelity, showcasing significant improvements in detail, composition, and text rendering.

Table 1. **Computational Cost Comparison.** We report the total NVIDIA H100 GPU hours for the fine-tuning stage. Our CRAFT framework demonstrates a dramatic reduction in computational cost, achieving significant speedups over all baselines.

SDXL				SD1.5			
Method	Data	GPU Hours	Cost Ratio	Method	Data	GPU Hours	Cost Ratio
Diff-DPO	851,293	~638.1	159.5×	Diff-DPO	851,293	~80.6	42.4×
MaPO	928,068	~545.6	136.4×	Diff-KTO	851,293	~415.6	218.7×
SmPO	851,293	~120.1	30.0×	SmPO	851,293	~27.6	14.5×
SPO	4,000	~63.0	15.8×	SPO	4,000	~22.0	11.6×
CRAFT (Ours)	100	~4.0	1.0×	CRAFT (Ours)	100	~1.9	1.0×

hours on SDXL and ~ 1.9 GPU hours on SD1.5. The “Cost Ratio” column in Table 1 quantifies this advantage precisely. On SDXL, CRAFT is 15.8 \times faster than SPO and up to 159.5 \times faster than Diff-DPO. The efficiency gains are even more pronounced on SD1.5, where CRAFT outperforms SPO by 11.6 \times and Diff-KTO by a staggering 218.7 \times .

These results confirm that CRAFT not only eliminates the dependency on large-scale preference data but also enables rapid and effective diffusion model alignment at a fraction of the computational cost of existing methods. We attribute this significant improvement in efficiency to the fundamental superiority of our CRAFT framework design.

Table 2. **Quantitative Results** of our **CRAFT** and other baselines for SDXL. We report the average reward scores of images generated on HPDv2, Parti-Prompt, and Pick-a-Pic datasets. The highest value is shown in **bold**, the second highest is underlined, and models marked with * are reproduced strictly following the official code and datasets.

Model	HPDv2				Parti-Prompt				Pick-a-Pic			
	HPSv2.1 ↑	AES ↑	ImgReward ↑	MPS ↑	HPSv2.1 ↑	AES ↑	ImgReward ↑	MPS ↑	HPSv2.1 ↑	AES ↑	ImgReward ↑	MPS ↑
SDXL	27.93	5.803	0.819	14.35	27.32	5.683	0.747	11.38	27.95	5.844	0.649	11.36
Diff-DPO	29.76	5.851	1.037	14.70	28.74	5.789	1.032	11.84	29.59	5.908	0.924	11.68
MaPO	29.05	5.925	0.925	14.46	28.03	5.851	0.864	11.46	28.88	6.001	0.794	11.33
SmPO*	31.40	5.950	1.081	14.89	30.03	5.890	<u>1.100</u>	11.96	31.03	6.000	0.984	11.73
SPO*	<u>32.32</u>	<u>6.015</u>	<u>1.103</u>	<u>15.36</u>	<u>30.54</u>	<u>5.940</u>	1.058	<u>12.16</u>	<u>31.69</u>	<u>6.068</u>	<u>1.023</u>	<u>12.13</u>
CRAFT(Ours)	32.67	6.031	1.312	15.62	31.10	5.976	1.252	12.41	32.18	6.080	1.308	12.53

Table 3. **Quantitative Results** of our **CRAFT** and other baselines for SD1.5. We report the average reward scores of images generated on HPDv2, Parti-Prompt, and Pick-a-Pic datasets. The highest value is shown in **bold**, the second highest is underlined, and models marked with * are reproduced strictly following the official code and datasets.

Model	HPDv2				Parti-Prompt				Pick-a-Pic			
	HPS v2.1 ↑	AES ↑	ImgReward ↑	MPS ↑	HPS v2.1 ↑	AES ↑	ImgReward ↑	MPS ↑	HPS v2.1 ↑	AES ↑	ImgReward ↑	MPS ↑
SD1.5	24.57	5.500	0.234	12.24	25.27	5.470	0.246	9.79	24.83	5.488	0.107	9.12
Diff-DPO	25.81	5.602	0.428	12.77	26.07	5.540	0.404	10.18	25.88	5.558	0.269	9.56
Diff-KTO	<u>28.56</u>	5.681	<u>0.740</u>	<u>13.12</u>	<u>28.10</u>	5.667	<u>0.641</u>	10.28	<u>28.10</u>	5.662	<u>0.624</u>	9.55
SmPO*	26.41	5.497	0.432	12.65	26.51	5.492	0.425	10.03	26.68	5.534	0.320	9.55
SPO*	28.17	5.758	0.578	13.01	27.78	5.718	0.531	<u>10.42</u>	27.78	5.794	0.399	<u>9.80</u>
CRAFT(Ours)	29.17	<u>5.699</u>	0.753	13.36	28.30	<u>5.685</u>	0.648	10.48	28.44	<u>5.701</u>	0.711	9.90

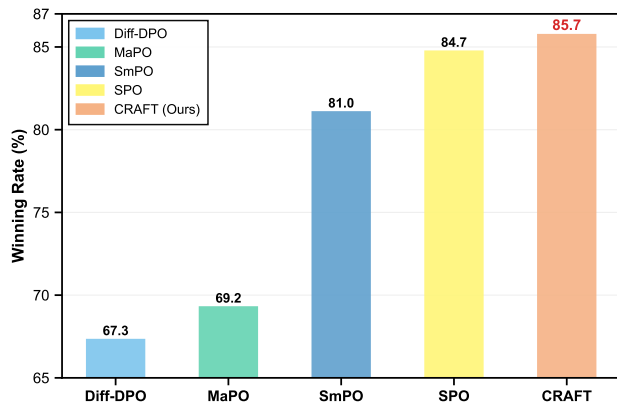


Figure 5. **Winning Rate Comparison on Parti-Prompt.** CRAFT outperforms all baseline methods in average winning rate against the base SDXL model.

Quantitative Results. Table 2 and Table 3 summarize the quantitative results of our proposed CRAFT and other baseline methods on SDXL and SD1.5. Each model is evaluated on three test sets: HPDv2, Parti-Prompt, and Pick-a-Pic, using HPSv2.1, AES, ImageReward and MPS. Overall, CRAFT consistently surpasses all baselines across nearly all evaluation metrics and datasets, demonstrating the effectiveness of our composite reward-based fine-tuning strat-

egy. A crucial indicator of our method’s generalization capability lies in its performance on metrics Image Reward (IR) and MPS, which are unseen during training. CRAFT demonstrates leading performance on these two metrics, providing compelling evidence that our alignment strategy generalizes effectively rather than merely overfitting to the training rewards. This is particularly evident on the HPDv2 benchmark with the SDXL model, where CRAFT not only attains the highest HPSv2.1 score (32.67) but also achieves the top IR score (1.312) and MPS score (15.62), outperforming the next-best method, SPO. This robust generalization is echoed in the SD1.5 model’s results, which leads with an HPSv2.1 of 29.17 and a superior MPS of 13.36. These consistent quantitative advantages are visualized in Figure 5, which illustrates CRAFT’s dominant average winning rate of over 85.7% on the Parti-Prompt dataset, underscoring its superior alignment with human preferences. To further assess compositional reasoning, Table 4 reports the results on the GenEval benchmark. These tests evaluate complex capabilities such as object counting, color and position binding, and attribute association. CRAFT achieves the best or second-best performance across most evaluation categories on SD1.5. This performance on compositional tasks further validates the robust generalization of CRAFT’s alignment capabilities beyond standard preference optimization metrics.

Table 4. **GenEval results** of our **CRAFT** and baseline methods for SD1.5. The highest value is shown in bold, the second highest is underlined, and models marked with * are reproduced strictly following the official code and datasets.

Method	Single	Two	Attribute				Overall
	Object	Object	Counting	Colors	Position	Binding	
SD1.5	95.62	39.14	<u>36.56</u>	74.47	3.50	5.25	42.42
Diff-DPO	98.12	38.38	35.00	<u>77.39</u>	4.75	6.00	43.28
SmPO*	96.25	41.92	32.19	75.53	4.00	<u>7.25</u>	42.86
SPO*	95.94	49.75	33.44	72.61	<u>6.25</u>	6.25	<u>44.04</u>
CRAFT	<u>96.88</u>	<u>47.22</u>	38.12	77.66	6.75	8.25	45.82

4.3. Ablation and Analysis

Table 5. **Data selection strategy comparison.** This table validates our data filtering approach, showing that a small but high-quality dataset is superior. The Top-100 strategy consistently achieves the best performance across all metrics, surpassing strategies that use significantly more, but lower-quality data.

Strategy	Setup		Scores		
	Data	Steps	HPS↑	AES↑	IR↑
All	2,312	1,000	32.20	6.08	0.987
Low	500	500	31.86	5.94	1.040
Rand	500	500	33.10	6.07	1.110
Top	100	200	33.23	6.13	1.138

Selecting Strategy. To evaluate the effectiveness of our composite reward filtering strategy, we conduct an ablation study on data selection. We begin with a set of 2,312 samples, which constitutes the entire dataset curated through our Composite Reward Filtering. We compare four selecting strategies: 1) All: training on all 2,312 samples; 2) Low: training on the 500 lowest-scoring samples; 3) Random: training on 500 randomly selected samples; and 4) Top: training on the 100 highest-scoring samples. Recognizing that larger datasets require more training steps to converge, we scaled the training duration for each strategy to ensure a fair comparison of their peak potential. We report the optimal results achieved for each configuration in Table 5. The results clearly demonstrate the superiority of our Top selection strategy. Despite using less than 5% of the data (100 samples) and lower training cost (200 steps), this strategy achieves the highest scores across all metrics, including an AES of 6.13 and a remarkable IR score of 1.138. Strikingly, this performance surpasses that of the All strategy trained for 1,000 steps. Conversely, training with the entire dataset yields one of the weakest performances. This strongly validates that meticulous selection of high-quality data is critical for achieving optimal model performance.

Composite Reward Models. To determine the optimal composition of our reward function, we conducted an ablation study on different reward model combinations, with results detailed in Table 6. Our analysis reveals that relying on a single reward model is suboptimal. Specifically, using HPS alone yields the weakest performance, while using PickScore alone proves significantly more effective. Interestingly, the combination of HPS and AES fails to surpass the performance of PickScore, underscoring its critical importance for data quality. Based on these insights, our final composite reward function is designed to heavily favor the most effective signals. We assign equal high weight to HPS and PickScore ($\alpha_h = \alpha_p = 0.4$), reflecting their complementary strengths in capturing human preference and text-image alignment, while assigning a smaller weight to AES ($\alpha_a = 0.2$), which primarily measures general aesthetics. The superior performance of this full combination, as shown in the final row, validates this principled weighting strategy and highlights that while the full combination is best, PickScore is the most crucial individual component.

Table 6. **Reward model combination ablation.** We evaluate the impact of different Composite Reward functions on fine-tuning SDXL. All images are generated with pick-a-pic test sets.

Reward Models			Performance Metrics		
HPS	AES	Pic	HPS↑	AES↑	IR↑
✓			30.25	5.94	0.791
		✓	31.71	6.04	0.973
✓	✓		30.93	6.00	0.834
✓	✓	✓	32.20	6.08	0.987

5. Conclusion

In this work, we address two key challenges in aligning diffusion models: data dependency and high computational cost. We introduce CRAFT, a simple yet effective framework that achieves strong generation alignment using only a handful of samples. CRAFT first constructs a high-quality dataset with a composite reward filtering strategy, and then fine-tunes diffusion models with a weighted supervised objective guided by composite reward. Theoretically, we prove that CRAFT can be viewed as a lower-bound optimization of group-based reinforcement learning, providing a principled link between supervised fine-tuning and reinforcement learning. Empirically, CRAFT fine-tunes SD1.5 and SDXL with only 100 samples, achieving up to 220× faster training while surpassing the alignment quality of existing methods. These results demonstrate that effective diffusion model alignment does not require massive datasets or computationally intensive optimization.

Acknowledgement. This work was supported by the National Natural Science Foundation of China under Grant No. 62506317.

References

- [1] Jinze Bai, Shuai Bai, Yunfei Chu, Zeyu Cui, Kai Dang, Xiaodong Deng, Yang Fan, Wenbin Ge, Yu Han, Fei Huang, et al. Qwen technical report. *arXiv preprint arXiv:2309.16609*, 2023. 5
- [2] Lichen Bai, Masashi Sugiyama, and Zeke Xie. Weak-to-strong diffusion with reflection. In *International Conference on Learning Representations*, 2026. 6
- [3] Kevin Black, Michael Janner, Yilun Du, Ilya Kostrikov, and Sergey Levine. Training diffusion models with reinforcement learning. *arXiv preprint arXiv:2305.13301*, 2023. 3
- [4] Ying Fan, Olivia Watkins, Yuqing Du, Hao Liu, Moonkyung Ryu, Craig Boutilier, Pieter Abbeel, Mohammad Ghavamzadeh, Kangwook Lee, and Kimin Lee. Dpok: Reinforcement learning for fine-tuning text-to-image diffusion models. *Advances in Neural Information Processing Systems*, 36:79858–79885, 2023. 3
- [5] Dhruva Ghosh, Hannaneh Hajishirzi, and Ludwig Schmidt. Geneval: An object-focused framework for evaluating text-to-image alignment. *Advances in Neural Information Processing Systems*, 36:52132–52152, 2023. 5
- [6] Jonathan Ho, Ajay Jain, and Pieter Abbeel. Denoising diffusion probabilistic models. *Advances in neural information processing systems*, 33:6840–6851, 2020. 1, 2, 3, 5
- [7] Jiwoo Hong, Sayak Paul, Noah Lee, Kashif Rasul, James Thorne, and Jongheon Jeong. Margin-aware preference optimization for aligning diffusion models without reference. In *First Workshop on Scalable Optimization for Efficient and Adaptive Foundation Models*, 2024. 5
- [8] Rui Huang, Shitong Shao, Zikai Zhou, Pukun Zhao, Hangyu Guo, Tian Ye, Lichen Bai, Shuo Yang, and Zeke Xie. Diffusion dataset condensation: Training your diffusion model faster with less data. *arXiv preprint arXiv:2507.05914*, 2025. 6
- [9] Tero Karras, Samuli Laine, and Timo Aila. A style-based generator architecture for generative adversarial networks. In *Proceedings of the IEEE/CVF conference on computer vision and pattern recognition*, pages 4401–4410, 2019. 2
- [10] Yuval Kirstain, Adam Polyak, Uriel Singer, Shahbuland Matiana, Joe Penna, and Omer Levy. Pick-a-pic: An open dataset of user preferences for text-to-image generation. *Advances in neural information processing systems*, 36:36652–36663, 2023. 4, 5
- [11] Black Forest Labs, Stephen Batifol, Andreas Blattmann, Frederic Boesel, Saksham Consul, Cyril Diagne, Tim Dockhorn, Jack English, Zion English, Patrick Esser, et al. Flux. 1 kontext: Flow matching for in-context image generation and editing in latent space. *arXiv preprint arXiv:2506.15742*, 2025. 1
- [12] Bao Li, Zeke Xie, Xiaomei Zhang, Xiangyu Zhu, and Zhen Lei. Diffusion models are zero-shot generative text-vision retrievers. In *ICASSP 2025 - 2025 IEEE International Conference on Acoustics, Speech and Signal Processing (ICASSP)*, pages 1–5, 2025. 6
- [13] Haopeng Li, Shitong Shao, Wenliang Zhong, Zikai Zhou, Lichen Bai, Hui Xiong, and Zeke Xie. Pisa: Piecewise sparse attention is wiser for efficient diffusion transformers. *arXiv preprint arXiv:2602.01077*, 2026. 6
- [14] Shufan Li, Konstantinos Kallidromitis, Akash Gokul, Yusuke Kato, and Kazuki Kozuka. Aligning diffusion models by optimizing human utility. *Advances in Neural Information Processing Systems*, 37:24897–24925, 2024. 3, 5
- [15] Zhanhao Liang, Yuhui Yuan, Shuyang Gu, Bohan Chen, Tiankai Hang, Mingxi Cheng, Ji Li, and Liang Zheng. Aesthetic post-training diffusion models from generic preferences with step-by-step preference optimization. In *Proceedings of the Computer Vision and Pattern Recognition Conference*, pages 13199–13208, 2025. 1, 3, 5
- [16] Buhua Liu, Shitong Shao, Bao Li, Lichen Bai, Zhiqiang Xu, Haoyi Xiong, James T Kwok, Sumi Helal, and Zeke Xie. Alignment of diffusion models: Fundamentals, challenges, and future. *ACM Computing Surveys*, 58(9):1–37, 2026. 2, 6
- [17] Jie Liu, Gongye Liu, Jiajun Liang, Yangguang Li, Jiaheng Liu, Xintao Wang, Pengfei Wan, Di Zhang, and Wanli Ouyang. Flow-grpo: Training flow matching models via online rl. *arXiv preprint arXiv:2505.05470*, 2025. 3
- [18] Ilya Loshchilov and Frank Hutter. Decoupled weight decay regularization. *arXiv preprint arXiv:1711.05101*, 2017. 5
- [19] Yunhong Lu, Qichao Wang, Hengyuan Cao, Xiaoyin Xu, and Min Zhang. Smoothed preference optimization via renoise inversion for aligning diffusion models with varied human preferences. *arXiv preprint arXiv:2506.02698*, 2025. 1, 3, 5
- [20] Long Ouyang, Jeffrey Wu, Xu Jiang, Diogo Almeida, Carroll Wainwright, Pamela Mishkin, Chong Zhang, Sandhini Agarwal, Katarina Slama, Alex Ray, et al. Training language models to follow instructions with human feedback. *Advances in neural information processing systems*, 35:27730–27744, 2022. 1
- [21] Dustin Podell, Zion English, Kyle Lacey, Andreas Blattmann, Tim Dockhorn, Jonas Müller, Joe Penna, and Robin Rombach. Sdxl: Improving latent diffusion models for high-resolution image synthesis. *arXiv preprint arXiv:2307.01952*, 2023. 1, 3
- [22] Zipeng Qi, Lichen Bai, Haoyi Xiong, and Zeke Xie. Not all noises are created equally: Diffusion noise selection and optimization. In *IEEE International Conference on Multimedia and Expo*, 2026. 6
- [23] Zipeng Qi, Buhua Liu, Lichen Bai, Zhiqiang Xu, Hu Yang, Haoyi Xiong, and Zeke Xie. A simple and efficient baseline for zero-shot generative classification. In *IEEE International Conference on Multimedia and Expo*, 2026. 6
- [24] Rafael Rafailov, Archit Sharma, Eric Mitchell, Christopher D Manning, Stefano Ermon, and Chelsea Finn. Direct preference optimization: Your language model is secretly a reward model. *Advances in neural information processing systems*, 36:53728–53741, 2023. 1, 3, 5
- [25] Aditya Ramesh, Mikhail Pavlov, Gabriel Goh, Scott Gray, Chelsea Voss, Alec Radford, Mark Chen, and Ilya Sutskever. Zero-shot text-to-image generation. In *International confer-*

- ence on machine learning, pages 8821–8831. Pmlr, 2021. 1, 2
- [26] Scott Reed, Zeynep Akata, Xinchun Yan, Lajanugen Logeswaran, Bernt Schiele, and Honglak Lee. Generative adversarial text to image synthesis. In *International conference on machine learning*, pages 1060–1069. Pmlr, 2016. 2
- [27] Robin Rombach, Andreas Blattmann, Dominik Lorenz, Patrick Esser, and Björn Ommer. High-resolution image synthesis with latent diffusion models. In *Proceedings of the IEEE/CVF conference on computer vision and pattern recognition*, pages 10684–10695, 2022. 1, 3
- [28] Chitwan Saharia, William Chan, Saurabh Saxena, Lala Li, Jay Whang, Emily L Denton, Kamyar Ghasemipour, Raphael Gontijo Lopes, Burcu Karagol Ayan, Tim Salimans, et al. Photorealistic text-to-image diffusion models with deep language understanding. *Advances in neural information processing systems*, 35:36479–36494, 2022. 1, 2
- [29] Christoph Schuhmann, Romain Beaumont, Richard Vencu, Cade Gordon, Ross Wightman, Mehdi Cherti, Theo Coombes, Aarush Katta, Clayton Mullis, Mitchell Wortsman, et al. Laion-5b: An open large-scale dataset for training next generation image-text models. *Advances in Neural Information Processing Systems*, 35:25278–25294, 2022. 1, 3, 4, 5
- [30] Shitong Shao, Zikai Zhou, Tian Ye, Lichen Bai, Zhiqiang Xu, and Zeke Xie. Bag of design choices for inference of high-resolution masked generative transformer. *arXiv preprint arXiv:2411.10781*, 2024. 6
- [31] Shitong Shao, Hongwei Yi, Hanzhong Guo, Tian Ye, Daquan Zhou, Michael Lingelbach, Zhiqiang Xu, and Zeke Xie. Magicdistillation: Weak-to-strong video distillation for large-scale few-step synthesis. *arXiv preprint arXiv:2503.13319*, 2025. 6
- [32] Shitong Shao, Zikai Zhou, Lichen Bai, Haoyi Xiong, and Zeke Xie. Iv-mixed sampler: Leveraging image diffusion model for enhanced video synthesis. In *International Conference on Learning Representations*, 2025. 6
- [33] Shitong Shao, Zikai Zhou, Dian Xie, Yuetong Fang, Tian Ye, Lichen Bai, Bo Han, and Zeke Xie. Improved and accelerated text-to-image generation with collect, reflect, and refine. *IEEE Transactions on Pattern Analysis and Machine Intelligence*, 2026. 6
- [34] Zhihong Shao, Peiyi Wang, Qihao Zhu, Runxin Xu, Junxiao Song, Xiao Bi, Haowei Zhang, Mingchuan Zhang, YK Li, Yang Wu, et al. Deepseekmath: Pushing the limits of mathematical reasoning in open language models. *arXiv preprint arXiv:2402.03300*, 2024. 3
- [35] Yang Song and Stefano Ermon. Improved techniques for training score-based generative models. *Advances in neural information processing systems*, 33:12438–12448, 2020. 2
- [36] Yang Song, Jascha Sohl-Dickstein, Diederik P Kingma, Abhishek Kumar, Stefano Ermon, and Ben Poole. Score-based generative modeling through stochastic differential equations. *arXiv preprint arXiv:2011.13456*, 2020. 1, 2
- [37] Bram Wallace, Meihua Dang, Rafael Rafailov, Linqi Zhou, Aaron Lou, Senthil Purushwalkam, Stefano Ermon, Caiming Xiong, Shafiq Joty, and Nikhil Naik. Diffusion model alignment using direct preference optimization. In *Proceedings of the IEEE/CVF Conference on Computer Vision and Pattern Recognition*, pages 8228–8238, 2024. 1, 3
- [38] Jason Wei, Maarten Bosma, Vincent Y Zhao, Kelvin Guu, Adams Wei Yu, Brian Lester, Nan Du, Andrew M Dai, and Quoc V Le. Finetuned language models are zero-shot learners. *arXiv preprint arXiv:2109.01652*, 2021. 1
- [39] Xiaoshi Wu, Yiming Hao, Keqiang Sun, Yixiong Chen, Feng Zhu, Rui Zhao, and Hongsheng Li. Human preference score v2: A solid benchmark for evaluating human preferences of text-to-image synthesis. *arXiv preprint arXiv:2306.09341*, 2023. 4, 5
- [40] Dian Xie, Shitong Shao, Lichen Bai, Zikai Zhou, Bojun Cheng, Shuo Yang, Jun Wu, and Zeke Xie. Guidance matters: Rethinking the evaluation pitfall for text-to-image generation. In *International Conference on Learning Representations*, 2026. 6
- [41] Jiazheng Xu, Xiao Liu, Yuchen Wu, Yuxuan Tong, Qinkai Li, Ming Ding, Jie Tang, and Yuxiao Dong. Imagereward: Learning and evaluating human preferences for text-to-image generation. *Advances in Neural Information Processing Systems*, 36, 2024. 5
- [42] Zeyue Xue, Jie Wu, Yu Gao, Fangyuan Kong, Lingting Zhu, Mengzhao Chen, Zhiheng Liu, Wei Liu, Qiushan Guo, Weilin Huang, et al. Dancegrpo: Unleashing grpo on visual generation. *arXiv preprint arXiv:2505.07818*, 2025. 3
- [43] Ling Yang, Zhilong Zhang, Yang Song, Shenda Hong, Runsheng Xu, Yue Zhao, Wentao Zhang, Bin Cui, and Ming-Hsuan Yang. Diffusion models: A comprehensive survey of methods and applications. *ACM computing surveys*, 56(4): 1–39, 2023. 2, 3
- [44] Shuo Yang, Zeke Xie, Hanyu Peng, Min Xu, Mingming Sun, and Ping Li. Dataset pruning: Reducing training data by examining generalization influence. In *International Conference on Learning Representations*, 2023. 6
- [45] Jiahui Yu, Yuanzhong Xu, Jing Yu Koh, Thang Luong, Gungjan Baid, Zirui Wang, Vijay Vasudevan, Alexander Ku, Yinfei Yang, Burcu Karagol Ayan, et al. Scaling autoregressive models for content-rich text-to-image generation. *arXiv preprint arXiv:2206.10789*, 2(3):5, 2022. 5
- [46] Sixian Zhang, Bohan Wang, Junqiang Wu, Yan Li, Tingting Gao, Di Zhang, and Zhongyuan Wang. Learning multi-dimensional human preference for text-to-image generation. In *Proceedings of the IEEE/CVF Conference on Computer Vision and Pattern Recognition*, pages 8018–8027, 2024. 5
- [47] Zikai Zhou, Shitong Shao, Lichen Bai, Shufei Zhang, Zhiqiang Xu, Bo Han, and Zeke Xie. Golden noise for diffusion models: A learning framework. In *Proceedings of the IEEE/CVF International Conference on Computer Vision*, pages 17688–17697, 2025. 6
- [48] Huaisheng Zhu, Teng Xiao, and Vasant G Honavar. DSPO: Direct score preference optimization for diffusion model alignment. In *The Thirteenth International Conference on Learning Representations*, 2025. 3, 4

CRAFT: Aligning Diffusion Models with Fine-Tuning Is Easier Than You Think

Supplementary Material

A. Detailed Proof of Theorem 3.1

We provide a fully detailed derivation of the proposed lower bound for clarity.

Step 0: Restate the empirical objective.

Recall the empirical Monte Carlo objective:

$$\hat{J}(\theta) = \mathbb{E}_{\mathbf{c} \sim \mathcal{D}_c, \{\mathbf{x}_0^{(i)}\}_{i=1}^G \sim p_{\theta_{\text{old}}}(\cdot|\mathbf{c})} \left[\frac{1}{G} \sum_{i=1}^G \frac{p_{\theta}(\mathbf{x}_0^{(i)}|\mathbf{c})}{p_{\theta_{\text{old}}}(\mathbf{x}_0^{(i)}|\mathbf{c})} \cdot \hat{A}_i \right], \quad (5)$$

where

$$\hat{A}_i = \frac{r(\mathbf{c}, \mathbf{x}_0^{(i)}) - \text{mean}\{r(\mathbf{c}, \mathbf{x}_0^{(1)}), \dots, r(\mathbf{c}, \mathbf{x}_0^{(G)})\}}{\text{std}\{r(\mathbf{c}, \mathbf{x}_0^{(1)}), \dots, r(\mathbf{c}, \mathbf{x}_0^{(G)})\} + \epsilon}, \quad \frac{1}{G} \sum_{i=1}^G \hat{A}_i = 0. \quad (6)$$

Step 1: Express in terms of log-likelihood difference.

Define the log-likelihood difference:

$$\Delta_i(\theta) := \log p_{\theta}(\mathbf{x}_0^{(i)}|\mathbf{c}) - \log p_{\theta_{\text{old}}}(\mathbf{x}_0^{(i)}|\mathbf{c}). \quad (7)$$

Then (5) becomes

$$\hat{J}(\theta) = \mathbb{E}_{\mathbf{c} \sim \mathcal{D}_c, \{\mathbf{x}_0^{(i)}\}_{i=1}^G \sim p_{\theta_{\text{old}}}(\cdot|\mathbf{c})} \left[\frac{1}{G} \sum_{i=1}^G \exp(\Delta_i(\theta)) \cdot \hat{A}_i \right]. \quad (8)$$

Step 2: ELBO form for diffusion models.

Now according to the evidence lower bound (ELBO) of the log-likelihood in diffusion models [6], we have

$$\begin{aligned} \log p_{\theta}(\mathbf{x}_0^{(i)}|\mathbf{c}) &= \log \int p_{\theta}(\mathbf{x}_{0:T}^{(i)}|\mathbf{c}) d\mathbf{x}_{1:T}^{(i)} \\ &= \log \int q(\mathbf{x}_{1:T}^{(i)}|\mathbf{x}_0^{(i)}) \frac{p_{\theta}(\mathbf{x}_{0:T}^{(i)}|\mathbf{c})}{q(\mathbf{x}_{1:T}^{(i)}|\mathbf{x}_0^{(i)})} d\mathbf{x}_{1:T}^{(i)} \\ &\geq \mathbb{E}_{q(\mathbf{x}_{1:T}^{(i)}|\mathbf{x}_0^{(i)})} \left[\log \frac{p_{\theta}(\mathbf{x}_{0:T}^{(i)}|\mathbf{c})}{q(\mathbf{x}_{1:T}^{(i)}|\mathbf{x}_0^{(i)})} \right] \\ &= - \mathbb{E}_{\substack{t \sim \text{Uniform}(\{1, \dots, T\}) \\ \boldsymbol{\epsilon}_t^{(i)} \sim \mathcal{N}(0, I)}} \left[\underbrace{\frac{1}{2\sigma_t^2} \cdot \frac{1 - \bar{\alpha}_t}{\bar{\alpha}_t}}_{w(t)} \cdot \left\| \boldsymbol{\epsilon}_{\theta}(\mathbf{x}_t^{(i)}, t, \mathbf{c}) - \boldsymbol{\epsilon}_t^{(i)} \right\|^2 \right] + \text{const}. \end{aligned} \quad (9)$$

So we can simply denote

$$\log p_{\theta}(\mathbf{x}_0^{(i)}|\mathbf{c}) = - \mathbb{E}_{\substack{t \sim \text{Uniform}(\{1, \dots, T\}) \\ \boldsymbol{\epsilon}_t^{(i)} \sim \mathcal{N}(0, I)}} \left[w(t) \cdot \left\| \boldsymbol{\epsilon}_{\theta}(\mathbf{x}_t^{(i)}, t, \mathbf{c}) - \boldsymbol{\epsilon}_t^{(i)} \right\|^2 \right] + C_i, \quad (10)$$

where C_i does not depend on θ . Similarly, for the old parameters:

$$\log p_{\theta_{\text{old}}}(\mathbf{x}_0^{(i)}|\mathbf{c}) = - \mathbb{E}_{\substack{t \sim \text{Uniform}(\{1, \dots, T\}) \\ \boldsymbol{\epsilon}_t^{(i)} \sim \mathcal{N}(0, I)}} \left[w(t) \cdot \left\| \boldsymbol{\epsilon}_{\theta_{\text{old}}}(\mathbf{x}_t^{(i)}, t, \mathbf{c}) - \boldsymbol{\epsilon}_t^{(i)} \right\|^2 \right] + C'_i, \quad (11)$$

Subtracting gives the exact identity:

$$\Delta_i(\theta) = - \mathbb{E}_{\substack{t \sim \text{Uniform}(\{1, \dots, T\}) \\ \epsilon_t^{(i)} \sim \mathcal{N}(0, I)}} \left[w(t) \cdot \left(\left\| \epsilon_{\theta_{\text{old}}}(\mathbf{x}_t^{(i)}, t, \mathbf{c}) - \epsilon_t^{(i)} \right\|^2 - \left\| \epsilon_{\theta}(\mathbf{x}_t^{(i)}, t, \mathbf{c}) - \epsilon_t^{(i)} \right\|^2 \right) \right] + C_i - C'_i. \quad (12)$$

Define

$$M_i^\theta := \mathbb{E}_{\substack{t \sim \text{Uniform}(\{1, \dots, T\}) \\ \epsilon_t^{(i)} \sim \mathcal{N}(0, I)}} \left[w(t) \cdot \left\| \epsilon_{\theta}(\mathbf{x}_t^{(i)}, t, \mathbf{c}) - \epsilon_t^{(i)} \right\|^2 \right], \quad M_i^{\theta_{\text{old}}} := \mathbb{E}_{\substack{t \sim \text{Uniform}(\{1, \dots, T\}) \\ \epsilon_t^{(i)} \sim \mathcal{N}(0, I)}} \left[w(t) \cdot \left\| \epsilon_{\theta_{\text{old}}}(\mathbf{x}_t^{(i)}, t, \mathbf{c}) - \epsilon_t^{(i)} \right\|^2 \right]. \quad (13)$$

Then $\Delta_i(\theta) = -M_i^\theta + M_i^{\theta_{\text{old}}} + C_i - C'_i$.

Step 3: Factor out constants.

The term $C_i - C'_i$ does not depend on θ , so

$$\exp(\Delta_i(\theta)) = \exp(C_i - C'_i) \cdot \exp(-M_i^\theta + M_i^{\theta_{\text{old}}}), \quad (14)$$

where $\exp(C_i - C'_i)$ can be absorbed into a constant \tilde{C} . Hence

$$\hat{J}(\theta) = \tilde{C} + \mathbb{E}_{\mathbf{c} \sim \mathcal{D}_{\mathbf{c}}, \{\mathbf{x}_0^{(i)}\}_{i=1}^G \sim p_{\theta_{\text{old}}}(\cdot | \mathbf{c})} \left[\frac{1}{G} \sum_{i=1}^G \exp(-M_i^\theta + M_i^{\theta_{\text{old}}}) \cdot \hat{A}_i \right]. \quad (15)$$

Step 4: Taylor expansion via small learning rate.

Assume $\theta = \theta_{\text{old}} + \eta g$, with $\eta \rightarrow 0$. The noise predictor ϵ_{θ} is a smooth function of θ , so we can do a first-order Taylor expansion, i.e., $f(\theta_{\text{old}} + \eta g) = f(\theta_{\text{old}}) + \eta \nabla_{\theta} f(\theta_{\text{old}}) \cdot g + O(\eta^2)$, we have

$$\epsilon_{\theta}(\mathbf{x}_t^{(i)}, t, \mathbf{c}) = \epsilon_{\theta_{\text{old}}}(\mathbf{x}_t^{(i)}, t, \mathbf{c}) + \eta \nabla_{\theta} \epsilon_{\theta}(\mathbf{x}_t^{(i)}, t, \mathbf{c})|_{\theta_{\text{old}}} \cdot g + O(\eta^2). \quad (16)$$

Thus the difference

$$\epsilon_{\theta}(\mathbf{x}_t^{(i)}, t, \mathbf{c}) - \epsilon_{\theta_{\text{old}}}(\mathbf{x}_t^{(i)}, t, \mathbf{c}) = O(\eta). \quad (17)$$

Consequently, the squared error inside M_i^θ can be expanded:

$$\begin{aligned} & \left\| \epsilon_{\theta}(\mathbf{x}_t^{(i)}, t, \mathbf{c}) - \epsilon_t^{(i)} \right\|^2 \\ &= \left\| \epsilon_{\theta}(\mathbf{x}_t^{(i)}, t, \mathbf{c}) - \epsilon_{\theta_{\text{old}}}(\mathbf{x}_t^{(i)}, t, \mathbf{c}) + \epsilon_{\theta_{\text{old}}}(\mathbf{x}_t^{(i)}, t, \mathbf{c}) - \epsilon_t^{(i)} \right\|^2 \\ &= \left\| \epsilon_{\theta_{\text{old}}}(\mathbf{x}_t^{(i)}, t, \mathbf{c}) - \epsilon_t^{(i)} \right\|^2 + 2 \left(\epsilon_{\theta_{\text{old}}}(\mathbf{x}_t^{(i)}, t, \mathbf{c}) - \epsilon_t^{(i)} \right)^{\top} \left(\epsilon_{\theta}(\mathbf{x}_t^{(i)}, t, \mathbf{c}) - \epsilon_{\theta_{\text{old}}}(\mathbf{x}_t^{(i)}, t, \mathbf{c}) \right) + O(\eta^2). \end{aligned} \quad (18)$$

Taking expectation over t and $\epsilon_t^{(i)}$ gives

$$M_i^\theta = M_i^{\theta_{\text{old}}} + O(\eta) \implies M_i^\theta - M_i^{\theta_{\text{old}}} = O(\eta), \quad (19)$$

justifying the linearization:

$$\exp(-M_i^\theta + M_i^{\theta_{\text{old}}}) = \exp\left(-\left(M_i^\theta - M_i^{\theta_{\text{old}}}\right)\right) = 1 - \left(M_i^\theta - M_i^{\theta_{\text{old}}}\right) + O(\eta^2). \quad (20)$$

Step 6: Substitute back $\exp(-M_i^\theta + M_i^{\theta_{\text{old}}})$ **in terms of diffusion MSE.**

Finally,

$$\begin{aligned}
\hat{J}(\theta) &= \tilde{C} + \mathbb{E}_{\mathbf{c} \sim \mathcal{D}_{\mathbf{c}}, \{\mathbf{x}_0^{(i)}\}_{i=1}^G \sim p_{\theta_{\text{old}}}(\cdot|\mathbf{c})} \left[\frac{1}{G} \sum_{i=1}^G \exp(-M_i^\theta + M_i^{\theta_{\text{old}}}) \cdot \hat{A}_i \right] \\
&= \tilde{C} + \mathbb{E}_{\mathbf{c} \sim \mathcal{D}_{\mathbf{c}}, \{\mathbf{x}_0^{(i)}\}_{i=1}^G \sim p_{\theta_{\text{old}}}(\cdot|\mathbf{c})} \left[\frac{1}{G} \sum_{i=1}^G \left(1 - (M_i^\theta - M_i^{\theta_{\text{old}}}) + O(\eta^2) \right) \cdot \hat{A}_i \right] \\
&= \underbrace{\tilde{C} + \mathbb{E}_{\mathbf{c} \sim \mathcal{D}_{\mathbf{c}}, \{\mathbf{x}_0^{(i)}\}_{i=1}^G \sim p_{\theta_{\text{old}}}(\cdot|\mathbf{c})} \left[\frac{1}{G} \sum_{i=1}^G \hat{A}_i \right]}_{=0} + \underbrace{\mathbb{E}_{\mathbf{c} \sim \mathcal{D}_{\mathbf{c}}, \{\mathbf{x}_0^{(i)}\}_{i=1}^G \sim p_{\theta_{\text{old}}}(\cdot|\mathbf{c})} \left[\frac{1}{G} \sum_{i=1}^G M_i^{\theta_{\text{old}}} \cdot \hat{A}_i \right]}_{\text{constant}} \\
&\quad - \mathbb{E}_{\mathbf{c} \sim \mathcal{D}_{\mathbf{c}}, \{\mathbf{x}_0^{(i)}\}_{i=1}^G \sim p_{\theta_{\text{old}}}(\cdot|\mathbf{c})} \left[\frac{1}{G} \sum_{i=1}^G M_i^\theta \cdot \hat{A}_i \right] + O(\eta^2),
\end{aligned} \tag{21}$$

substituting the definition of M_i^θ , we have

$$\hat{J}(\theta) \geq C - \mathbb{E}_{\substack{\mathbf{c} \sim \mathcal{D}_{\mathbf{c}}, \\ \{\mathbf{x}_0^{(i)}\}_{i=1}^G \sim p_{\theta_{\text{old}}}(\cdot|\mathbf{c}), \\ t \sim \text{Uniform}(\{1, \dots, T\}) \\ \epsilon_t^{(i)} \sim \mathcal{N}(0, I)}} \left[\frac{1}{G} \sum_{i=1}^G \hat{A}_i w(t) \cdot \left\| \epsilon_\theta(\mathbf{x}_t^{(i)}, t, \mathbf{c}) - \epsilon_t^{(i)} \right\|^2 \right]. \tag{22}$$

This completes the proof.

B. Supplementary Experimental Results

Evaluation Bias on PicScore. In this work, we exclude PickScore from our primary evaluation metrics to ensure a fair and unbiased comparison. Most state-of-the-art baselines (e.g., Diff-DPO, SPO, SmPO) are explicitly optimized using the Pick-a-Pic dataset. Since the PickScore evaluator is trained on the exact same preference distribution, using it to evaluate these methods introduces significant **in-domain bias**, where high scores may reflect dataset overfitting rather than generalized generation quality. To avoid this data leakage and demonstrate the robustness of our method, we adopt a comprehensive suite of four independent metrics: **HPSv2.1**, **ImageReward**, **Aesthetic Score (AES)**, and **MPS**. These evaluators are derived from diverse data sources distinct from the baselines’ training sets, providing a neutral ground for comparison. By validating our approach across this multi-dimensional framework, we ensure that the reported performance reflects genuine improvements in human alignment and aesthetic quality, fully substantiating the effectiveness of our method without relying on potentially biased indicators.

General Results on SDXL. We extend our evaluation to the larger SDXL architecture to verify the scalability and effectiveness of our method. As presented in Table 12, **CRAFT** achieves the highest ‘Overall’ score of **57.97**, surpassing the base SDXL model (55.05) as well as recent alignment baselines such as Diff-DPO (57.23) and SmPO (57.86). Notably, CRAFT demonstrates superior capability in ensuring object presence and spatial fidelity. It secures state-of-the-art results in the ‘Single Object’ (**99.06**) and ‘Two Object’ (**86.36**) categories. The significant margin in the ‘Two Object’ metric, outperforming the second-best method by nearly 6 points, highlights CRAFT’s robustness in complex multi-subject generation scenarios. Furthermore, CRAFT also leads in the ‘Position’ category with a score of **14.50**, while maintaining highly competitive performance in attribute binding and color consistency. These results confirm that CRAFT effectively enhances the controllability and compositional alignment of large-scale text-to-image models.

More Visualization. Figure 8 provide additional visually appealing samples generated by CRAFT-SDXL, showcasing both its general aesthetic superiority and its specific structural integrity. Consistent with the main text, the prompts for these images are sourced from the HPDv2, Parti-Prompt, and Pick-a-Pic test sets, affirming performance across diverse domains. Figure 6 includes results from ControlNet, demonstrating CRAFT’s superior control fidelity when guided by conditioning inputs



Figure 6. **ControlNet Visualization: Superior Control Fidelity and Data Efficiency of CRAFT.** Qualitative comparison using diverse ControlNet conditions (**Canny** and **Depth**) against existing fine-tuning methods (SDXL, Diff-DPO, MaPO, SmPO). CRAFT consistently demonstrates strong geometric control fidelity and generates visually superior images across all modalities. This high robustness and aesthetic quality are achieved despite utilizing significantly fewer training samples, highlighting CRAFT’s superior data efficiency and generalization capability.

Table 7. **End-to-end cost in H100 hours.** For CRAFT, we report both preprocessing and fine-tuning cost. Even with candidate generation and filtering included, CRAFT remains substantially more efficient than prior methods.

	SDXL			SD1.5	
Method	Hours	Ratio	Method	Hours	Ratio
Diff-DPO	~638.1	26.5×	Diff-DPO	~80.6	9.2×
MaPO	~545.6	22.6×	Diff-KTO	~415.6	47.2×
CRAFT	~(4.0 + 20.1)	1.0×	CRAFT	~(1.9 + 6.9)	1.0×

(such as Canny and Depth maps). These samples confirm the model’s robustness: the high aesthetic quality is consistently maintained even when the geometric structure is strictly constrained by external control signals, which is a key indicator of model generalization beyond simple style transfer.

End-to-End Efficiency. To provide a fairer efficiency comparison, we report the end-to-end cost of our pipeline, including candidate generation, reward-based filtering, and the final fine-tuning stage. As shown in Table 7, CRAFT remains substantially more efficient than existing baselines even after including preprocessing overhead. This is important because our method does not assume access to large-scale preference pairs; instead, it constructs a compact training set from prompts with a comparatively light self-curation stage.

Additional Preference-Optimization Baselines. We further compare CRAFT against recent preference-optimization baselines. Table 8 reports score-based comparisons against InPO using its public checkpoint. Table 9 summarizes the comparison against DSPO [48] using the reward win-rate statistics reported in its original paper, since official checkpoints are unavailable. Across all reported datasets and metrics, CRAFT remains consistently stronger.

Table 8. Comparison with InPO on SDXL.

Model	HPDv2			Parti-Prompt			Pick-a-Pic		
	HPS	AES	IR	HPS	AES	IR	HPS	AES	IR
InPO	30.79	5.837	1.058	29.27	5.756	1.024	30.30	5.870	0.978
CRAFT	32.67	6.031	1.312	31.10	5.976	1.252	32.18	6.080	1.308

Table 10. Vanilla SFT vs. CRAFT.

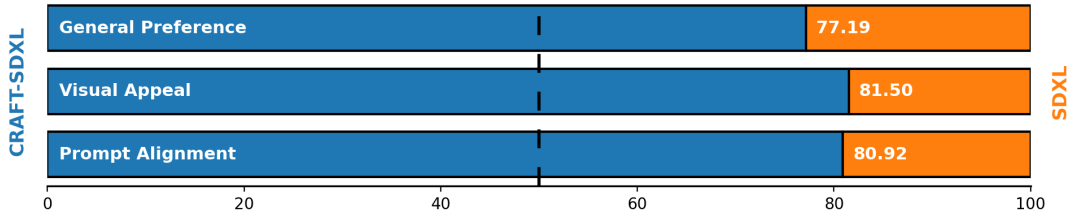
Method	HPS	AES	IR
Vanilla SFT	30.91	6.040	1.110
CRAFT	32.18	6.080	1.308

Table 9. Comparison with DSPO on SDXL.

Model	HPDv2			Parti-Prompt			Pick-a-Pic		
	HPS	AES	IR	HPS	AES	IR	HPS	AES	IR
DSPO	83.47	51.41	70.09	81.80	57.84	73.47	80.00	54.20	68.60
CRAFT	97.84	73.00	84.38	94.73	81.50	80.70	96.40	74.00	86.00

Table 11. T2I-CompBench.

Model	Attr. Bind.			Obj. Rela.		Complex
	C	S	T	Sp.	N-Sp.	
SD1.5	0.384	0.376	0.407	0.102	0.309	0.391
CRAFT	0.495	0.446	0.456	0.139	0.311	0.405

Figure 7. **User study results.** Human evaluation corroborates the automatic reward-based metrics and favors CRAFT over the compared baselines.

Isolating the Effect of Advantage Weighting. To separate the contribution of data selection from the contribution of the training objective, we train a vanilla SFT baseline on the exact same Top-100 filtered dataset used by CRAFT. Table 10 shows that advantage weighting yields clear gains over vanilla SFT, especially on HPS and ImageReward, demonstrating that the performance gain does not come solely from data filtering.

Human Evaluation and Semantic Faithfulness. Since pretrained reward models would be biased, we additionally report a user study in Figure 7. The human preference trend is consistent with our automatic evaluations, providing complementary evidence that the observed gains are not merely artifacts of the reward models. We also report T2I-CompBench in Table 11, which supports that prompt refinement does not degrade compositional or semantic faithfulness.

Prompt Refinement, Reward Balancing, and Dataset Diversity. We use Qwen-Plus to rewrite original prompt into several more descriptive variants, which are used only for candidate generation. Importantly, all reward computation and filtering are performed with respect to the original prompt, so candidates with semantic drift are naturally disfavored during selection. For composite reward filtering, we first map the three reward signals to comparable scales before applying the final weights (0.4, 0.4, 0.2) for HPS, PickScore, and AES. These coefficients should therefore be interpreted as relative importance weights rather than raw-scale coefficients. The ablation results in Table 6 indicate that the full combination is the most reliable in practice, while Table 5 shows that a compact Top-100 subset is sufficient for strong performance. In the final selected set, we did not observe exact duplicate prompts, and the strong performance across HPDv2, Parti-Prompt, Pick-a-Pic, GenEval, and T2I-CompBench suggests that the few-shot setting does not bias the model toward a narrow prompt pattern.

C. Discussion

Limitations. Despite the promising results achieved by CRAFT, we acknowledge two primary limitations in our current framework. First, regarding the algorithmic paradigm, CRAFT fundamentally operates as an offline Supervised Fine-Tuning approach. While efficient, it relies on a static dataset constructed prior to training. This formulation inherently limits the model’s data utilization efficiency and exploration capability compared to online Reinforcement Learning (RL) strategies (e.g., PPO or the recent GRPO), which can dynamically explore the generation space and potentially reach a higher performance ceiling. Second, regarding the data construction strategy, our current framework still selects training samples at the image level after generation, rather than explicitly modeling the quality of the initial noise itself. Recent studies suggest that

Table 12. **GenEval results** of our **CRAFT** and baseline methods for SDXL. The highest value is shown in bold, the second highest is underlined, and models marked with * are reproduced strictly following the official code and datasets.

Method	Single Object	Two Object	Counting	Colors	Position	Attribute Binding	Overall
SDXL	97.50	70.96	42.81	88.30	11.00	21.00	55.05
Diff-DPO	<u>98.75</u>	<u>80.56</u>	45.62	86.70	11.00	20.75	57.23
SmPO*	<u>98.75</u>	79.55	<u>44.69</u>	86.70	10.50	27.00	<u>57.86</u>
SPO*	97.81	80.05	38.44	84.04	<u>11.75</u>	20.50	55.43
CRAFT (Ours)	99.06	86.36	36.88	<u>87.23</u>	14.50	<u>23.75</u>	57.97

high-quality or prompt-aware noise can be selected, optimized, or learned to consistently improve sample quality [22, 47]. Incorporating such noise-aware criteria into our reward filtering pipeline is a promising yet currently unexplored direction. Third, regarding the application scope, our current experimental validation is exclusively confined to Text-to-Image (T2I) generation. Although the principles of preference-free alignment are theoretically universal, we have not yet addressed the unique challenges present in other modalities, such as the temporal consistency required for Text-to-Video (T2V) or the geometric constraints essential for Text-to-3D generation.

Future Directions. Building upon these observations, our future work will focus on three strategic expansions. To transcend the offline limitations, we aim to evolve CRAFT into an *online* learning framework. By implementing an iterative "generate-train" loop, we can continuously update the training data with the model's own evolving distributions. This on-policy approach will ensure the model receives sustained and increasingly precise gradient signals throughout the training process, bridging the gap between SFT and RL. We also plan to enrich our filtering stage with adaptive noise selection criteria, where the filtering form and quality standards can vary across prompts, models, or downstream objectives, potentially benefiting from learned noise priors and reflection-based sampling signals [2, 2, 22, 47]. Finally, to broaden the application scope, we plan to adapt the CRAFT algorithm to a wider array of generative tasks. Specifically, we will investigate how our composite reward filtering and fine-tuning can be integrated into T2V and T23D pipelines, exploring whether the robust alignment capabilities demonstrated in 2D images can effectively generalize to complex temporal and spatial dimensions. In particular, recent video inference and distillation techniques, such as weak-to-strong video distillation and mixed image-video samplers [31, 32], suggest that alignment-time fine-tuning and video-specific inference improvements may be fruitfully combined.

Broader Opportunities. Our work is also connected to several broader directions in the diffusion literature. A recent survey summarizes the fundamentals, challenges, and future directions of diffusion alignment [16]. From the data perspective, diffusion dataset condensation and dataset pruning suggest that compact yet informative training subsets can substantially reduce training cost [8, 44], which is consistent with our motivation of aligning models from extremely limited filtered data. From the evaluation perspective, recent work shows that T2I comparisons can be distorted by guidance-scale bias [40], reinforcing our use of multiple complementary metrics rather than relying on a single score. Meanwhile, CRAFT focuses on improving model alignment during fine-tuning, but it is naturally compatible with a range of orthogonal inference-time advances. Recent methods improve generation quality or efficiency through collect-reflect-refine pipelines, sparse attention approximations, or carefully designed inference heuristics for alternative generative backbones [13, 30, 33]. Beyond alignment and synthesis, diffusion models have also shown promise for zero-shot retrieval and classification [12, 23]. Understanding how these data-centric, inference-centric, and downstream semantic capabilities interact with preference-aligned diffusion models is another valuable direction for future research.

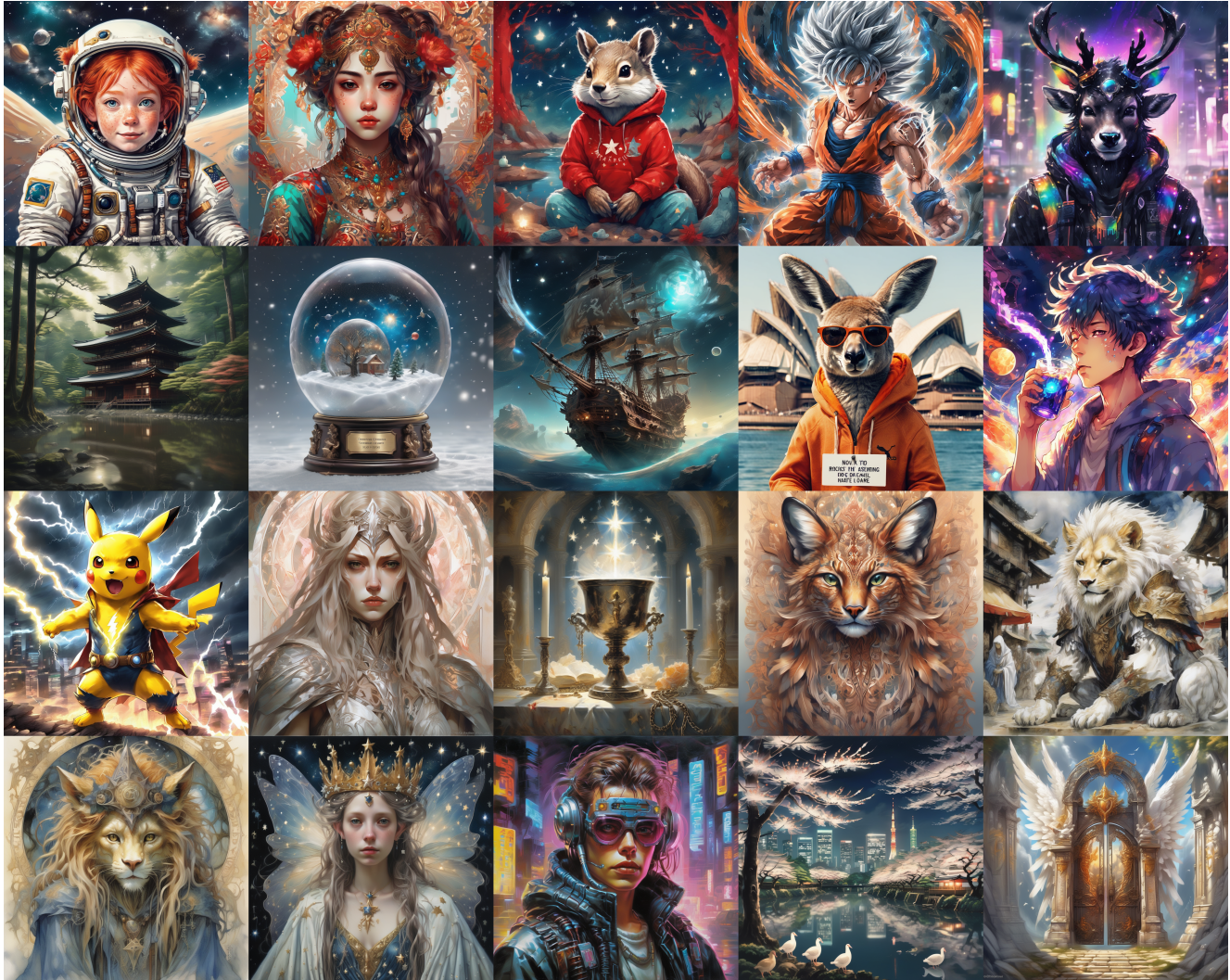


Figure 8. **Qualitative results of CRAFT-SDXL.** After CRAFT fine-tuning, the model demonstrates the capability to generate visually superior images with exceptional aesthetic quality.